Pre-Target Axon Sorting in the Avian Auditory Brainstem

Daniel T. Kashima, Edwin W Rubel, and Armin H. Seidl*

Virginia Merrill Bloedel Hearing Research Center, Department of Otolaryngology-Head and Neck Surgery, University of Washington, Seattle, Washington 98195-7923

ABSTRACT

Topographic organization of neurons is a hallmark of brain structure. The establishment of the connections between topographically organized brain regions has attracted much experimental attention, and it is widely accepted that molecular cues guide outgrowing axons to their targets in order to construct topographic maps. In a number of systems afferent axons are organized topographically along their trajectory as well, and it has been suggested that this pre-target sorting contributes to map formation. Neurons in auditory regions of the brain are arranged according to their best frequency (BF), the sound frequency they respond to optimally. This BF changes predictably with position along the so-called tonotopic axis. In the avian auditory brainstem, the tonotopic organization of the second- and third-order auditory neurons in nucleus magnocellularis (NM) and nucleus laminaris (NL) has been well described. In this study we examine whether the decussating NM axons forming the crossed dorsal cochlear tract (XDCT) and innervating the contralateral NL are arranged in a systematic manner. We electroporated dye into cells in different frequency regions of NM to anterogradely label their axons in XDCT. The placement of dye in NM was compared to the location of labeled axons in XDCT. Our results show that NM axons in XDCT are organized in a precise tonotopic manner along the rostrocaudal axis, spanning the entire rostrocaudal extent of both the origin and target nuclei. We propose that in the avian auditory brainstem, this pre-target axon sorting contributes to tonotopic map formation in NL. J. Comp. Neurol. 521:2310–2320, 2013.

INDEXING TERMS: axon topography; pre-target axon sorting; auditory system; tonotopic organization; sound localization

Topographic organization of neurons and their connections is a fundamental characteristic of the nervous system. Sensory modalities such as the retinotopic system and the somatotopic system depend on the presence of precise spatial organization of connections established and maintained from sensory receptors to higher order processing regions. In the same way, auditory centers in the brain are arranged topographically: the auditory sensory epithelium within the cochlea is arranged along a frequency gradient serving to separate sound into frequency components (Yates et al., 1992). In the auditory system of both birds and mammals, successive stages along ascending pathways from the cochlea maintain the neighbor relationships of the acoustic sensory epithelium (Schweitzer and Cant, 1984; Young and Rubel, 1986; Angulo et al., 1990; Snyder and Leake, 1997; for review, see Rubel and Fritzsch, 2002; Kandler et al., 2009). Specifically, the sound frequencies to which neurons in these cell groups respond best (best frequency [BF]) progressively and predictably shift with their anatomical position. Thus, these neurons are arranged along a gradient of frequency selectivity—or tonotopy. This organization differs from other sensory systems in that tonotopy is not present in nature; it is introduced by the cochlea.

The avian auditory brainstem is illustrated in a schematic depicting a coronal cross section of the neural circuit responsible for low-frequency sound localization (Fig. 1A). Excitatory activity from each ear is conveyed via the auditory nerves to the ipsilateral nucleus

D.T. Kashima's current address is Vanderbilt School of Medicine, Box 44, 215 Light Hall, Nashville, TN 37232.

Grant sponsors: the University of Washington Howard Hughes Medical Institute Integrative Research Internship Program (grant to D.T.K.); the University of Washington Mary Gates Research Scholarship (to D.T.K.); the University of Washington Levinson Emerging Scholars Program (grant to D.T.K.); National Institutes of Health; Grant number: DC011343, DC03829 and DC04661.

*CORRESPONDENCE TO: Armin H. Seidl, Virginia Merrill Bloedel Hearing Research Center, University of Washington, Box 357923, Seattle, WA 98195-7923. E-mail: armins@uw.edu

Received June 8, 2012; Revised December 4, 2012; Accepted December 11, 2012

DOI 10.1002/cne.23287

Published online December 14, 2012 in Wiley Online Library (wileyonlinelibrary.com)

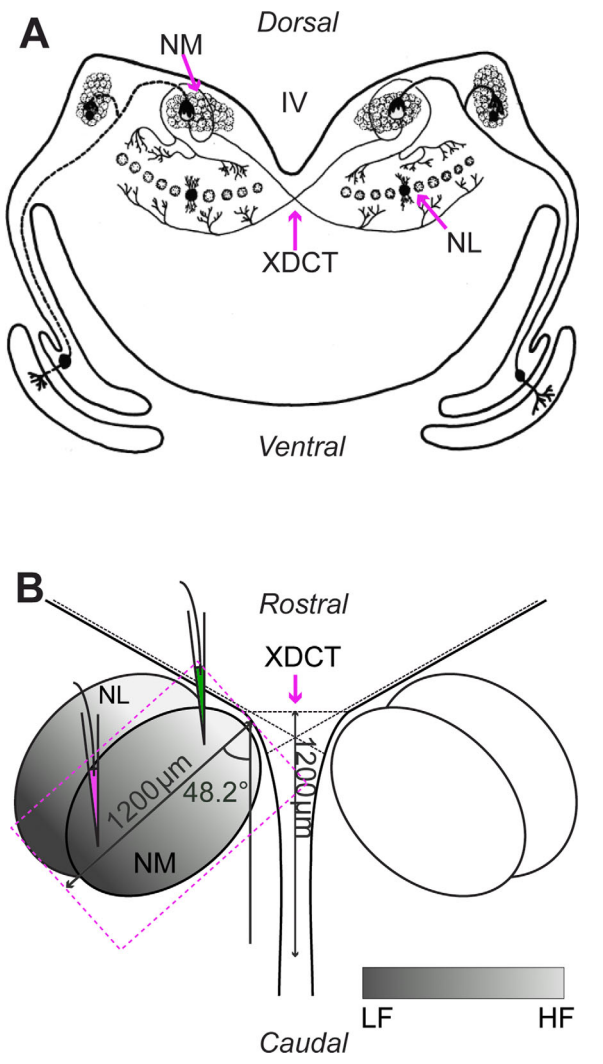

Figure 1. Schematic of avian sound localization circuit. **A**: Coronal view of circuit. Auditory signals are relayed via the 8th nerve to nucleus magnocellularis (NM). NM in turn sends out bifurcating axons terminating on the ipsi- and contralateral nucleus laminaris (NL). The projections crossing the midline form the crossed dorsal cochlear tract (XDCT). IV, 4th ventricle. Dorsal is up. **B**: Horizontal schematic illustrating the measurement parameters, tonotopy in NM and NL, and electroporation sites in different parts of NM along the tonotopic axis. For both structures, cells in the most rostromedial portions respond best to high-frequency (HF) sounds whereas more caudolateral areas respond best to progressively lower frequencies (LF). Fluorescence measurements of the injection sites were taken along a 1,200-µm rectangle encompassing the boundaries of NM beginning at the wall of the 4the ventricle and at a 48.2° angle relative to the midline. Measurements of filled XCDT axons were made along the midline beginning where the wall of the 4th ventricle begins to curve and ending 1,200 µm caudal from this point. Rostral is up, and dorsal faces the reader. [Color figure can be viewed in the online issue, which is available at wileyonlinelibrary.com.]

magnocellularis (NM), the first relay point for auditory signals in the avian brain (Boord and Rasmussen, 1963; Rubel and Parks, 1975; Parks and Rubel, 1978; Hackett et al., 1982; Jhaveri and Morest, 1982a; Carr and Konishi, 1990). Axons from NM neurons project bilaterally to nucleus laminaris (NL) (Parks and Rubel, 1975; Hackett et al., 1982; Young and Rubel, 1983; Carr and Konishi, 1990). Each NL neuron receives excitatory input from the ipsilateral and the contralateral NM, thereby receiving acoustic information from both ears. The axons from both NMs cross the midline, forming the crossed dorsal cochlear tract (XDCT) (Fig. 1A). Contralateral NM axons constitute a delay line onto the ventral side of NL (Fig. 1A) (Young and Rubel, 1983, 1986; Carr and Konishi, 1990; Joseph and Hyson, 1993). This circuit is considered to embody a modified Jeffress model for sound localization (Jeffress, 1948; Overholt et al., 1992; Seidl et al., 2010).

The neurons in both NM and NL are arranged in a precise tonotopic manner (Rubel and Parks, 1975). In both NM and NL, neurons with relatively high BFs are located in the rostromedial region, whereas neurons with progressively lower BFs are located in the progressively caudolateral region (Rubel and Parks, 1975; Lippe and Rubel, 1985; Fukui and Ohmori, 2004) (Fig. 1B). In addition to tonotopy of this circuit, cell morphology (Smith and Rubel, 1979; Jhaveri and Morest, 1982a,b), axonal arborizations (Young and Rubel, 1986; Seidl et al., 2010), and physiological properties (Fukui and Ohmori, 2004; Kuba et al., 2005) have been the subject of extensive research. Remarkably, these and many other properties display systematic spatial organizations correlating with the tonotopic map (Rubel and Parks, 1988; Nishino and Ohmori, 2009).

The purpose of this study was to examine the topographic organization of the NM axons in XDCT as they cross the midline. Previous studies in a variety of sensory and motor systems have shown an organization within axon tracts, but final refinement of projections is assumed to be dependent on molecular cues at the target region (reviewed by Flanagan, 2006; Feldheim and O'Leary, 2010). Because NM and NL are organized along a rostromedial–caudolateral tonotopy, we hypothesized that the organization of XDCT might follow a rostrocaudal tonotopic axis. We further hypothesized that this organization would not be precise; it would show examples of overlap and aberrant organization, consistent with the need for precise sorting at the target site, NL. We found that the position of labeled axons in XDCT was highly correlated with the position of the injection site along the tonotopic axis in NM, but without "mistakes" that we could identify. This supports our hypothesis that these axonal trajectories are tonotopically arranged, providing a highly accurate scaffold for the assembly of topographic connections, but does not support the assumption of a need for additional sorting to maintain tonotopy at the target.

MATERIALS AND METHODS

Whole-brainstem preparations of late-stage chicken embryos were explanted, and fluorescent dextrans of different colors were used to label small regions of NM at different regions along its tonotopic axis. Following the anterograde transport of the dyes along XDCT, the brainstem explants were fixed, cleared, and imaged. The rostrocaudal position of labeled axons in XDCT was quantified and compared with the location of the injection site.

Animals

A total of 92 white leghorn chicken (*Gallus gallus domesticus*) embryos of embryonic day 20 and E21 (E20, E21) were used, of which 19 were successfully labeled and subsequently analyzed for this study. Hearing onset in chickens is at E14–15 (Jackson and Rubel, 1978). Chickens hatch on E21, by which time the brainstem auditory responses to low frequencies mirror that of the adult bird (Saunders et al., 1973).

All procedures were approved by the University of Washington Institutional Animal Care and Use Committee and conformed to NIH guidelines.

Multicell electroporation

The embryo was removed from the egg and rapidly decapitated. The brain was extracted from the skull, the cerebellum was removed, and the whole-brain preparation containing the auditory brainstem was blocked and placed in a perfusion chamber with ice-cold oxygenated (95% O_2, 5% CO_2) artificial cerebral spinal fluid (ACSF; in mM: 130 NaCl, 3 KCl, 1.25 NaH_2PO_4, 26 $NaHCO_3$, 1 $MgCl_2$, 2 $CaCl_2$, and 10 glucose in filtered [18 MΩ] dH_2O) for 45 minutes (see Sanchez et al., 2011 for detailed description of procedure).

The electroporation method has been described in detail previously (Haas et al., 2001; Burger et al., 2005; Sorensen and Rubel, 2006; Seidl et al., 2010). Briefly, glass pipettes with a tip diameter of 0.5 μm were made with a vertical pipette puller (model 700B, David Kopf Instruments, Tujunga, CA). Tip shape and diameter were confirmed under a light microscope. The pipette was filled with a fluorescent dextran dye (Dextran, Alexa Fluor 488 or 568, D22910 or D22912, Molecular Probes, Grand Island, NY; 10 kDa MW; 20 mM in 0.9% NaCl solution) and connected to a Grass SD9 stimulator (Grass Technologies, West Warwick, RI) stimulator. Following a 45-minute period in cold ACSF, the brainstem was placed dorsal side up in petri dishes and partially covered with ACSF. Following visual identification of the location of NM, the dye-filled glass pipette was lowered into either the rostromedial region (high frequency [HF]) or a more caudolateral region (low frequency [LF]) of the left NM. The ground electrode was placed in the ACSF surrounding the brain. Dye was electroporated under visual control by passing 1-ms square voltage pulses (variable, set to cause a 1–3-μA current through the pipette tip) at 200 Hz through the glass pipette to deposit dye within NM cell bodies. For cases in which two dyes were injected, the process was repeated with a different colored dye, at a distinct tonotopic position in NM different from the first.

Following electroporation, the brainstem was incubated in oxygenated ACSF at room temperature (RT) for 3–4 hours in the dark to allow for anterograde dye transport along XDCT. Next, the brain was fixed in 4% paraformaldehyde for 15–30 minutes at RT, rinsed 3X 10 minutes in phosphate-buffered saline, and placed in 70% ethanol overnight at 4°C.

The fixed whole-brainstem preparation was then dehydrated by a series of ethanol steps and stored in a clearing solution (Spalteholz solution, 3:5 mixture of benzyl benzoate and methyl salicylate; adapted from MacDonald and Rubel, 2008; Seidl et al., 2010) at 4°C for at least 12 hours prior to imaging. This clearing technique allowed us to optically resolve filled axons deep into the tissue. No further physical sectioning occurred.

Imaging

In preparations in which injection site(s) and labeled NM axons along XDCT were identifiable, the whole-brainstem preparation was imaged from its dorsal side (same side the injection was made) by using an inverted FV-1000 confocal microscope (Olympus, Center Valley, PA). 3D image stacks from the whole brainstem were acquired

Data analysis and quantification

Measurements were conducted on maximum intensity projections made from the image stacks. Images were false colored and contrast enhanced by using Adobe Photoshop (San Jose, CA).

From a dorsal view, intensity measurements of dyes injected into NM were made along a 1,200-μm-long rectangular area from the wall of the 4th ventricle angled at a 48.2° angle from the midline (Fig. 1B). This is the angle at which the tonotopic axis of NM is located relative to the brainstem midline (Rubel and Parks, 1975; Lippe and Rubel, 1985). Fluorescent signal intensity was measured beginning at the edge of the 4th ventricle (corresponding to 0 μm) and was sampled every 3.11 μm caudolaterally for a total distance of 1,200 μm. This length of measurement was set to incorporate the extent of injection site(s). The width of the measured rectangular space was adjusted to incorporate the visible boundaries of NM.

The intensity values recorded along the tonotopic axis of each NM on the side of the injection(s) were normalized to span a range from 0 to 1. The center point of dye electroporation was defined as the absolute maximum in each intensity plot. Injection sizes were measured by examining the rostromedial to caudolateral distance for which the signal intensity surpassed the normalized value of 0.5. The percentage of overlap between the two injected dyes was determined by measuring the total distance along the NM tonotopic axis for which both dyes' signal intensity surpassed 0.5 and overlapped.

Fluorescence labeling intensity in XDCT was also sampled every 3.11 μm along a 1,200-μm length at the midline. These measurements began at the most anterior site where XDCT axons cross the midline, as determined from pilot studies labeling the most rostral pole of NM. This point is where the wall of the 4th ventricle begins to curve caudally (Fig. 1B). Signal maxima were verified by visually identifying corresponding labeled axons and measuring their location along the rostrocaudal dimension. The mean location of labeled axons along the rostrocaudal axis was calculated for each case in which two different colored dyes were electroporated. For all cases, these verified locations of single axons were recorded and compared with the corresponding center of NM injection location. For the correlation in Figure 6, we excluded datasets with an injection site that exceeded 25% of the length of the tonotopic axis in NM.

To analyze the correlation of single cell bodies and their contralateral axons (Fig. 7), we determined the relative distances between filled cell bodies along the tonotopic axis in NM (see above, Fig. 1B) and correlated them with the relative distance of their corresponding axons in XDCT along the rostrocaudal axis.

All statistical analyses were done with Prism 5 software (GraphPad Software, La Jolla, CA). Tests for statistical significance for data presented in Figure 5 were made by an unpaired *t*-test, and all error bars shown in figures represent the standard deviation (SD). We also performed a linear regression analysis and computed Pearson Product Moment correlations for the data presented in Figures 5–7.

RESULTS

NM axons project along distinct locations in XDCT

We compared the location of the NM injection site along the tonotopic axis with the distribution of labeled NM axons in XDCT along the rostrocaudal axis in an in vitro brainstem preparation. Figure 2 shows a maximum-intensity projection of a dorsal view from a representative example of a brainstem labeled with two different dyes.

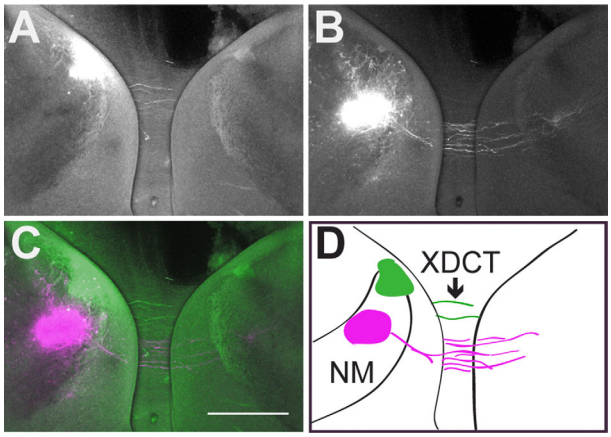

Figure 2. Two-dye electroporation into nucleus magnocellularis (NM). **A**: Maximum intensity projection of the green channel showing electroporation location into HF region of NM and filled axons. **B**: Maximum intensity projection of the red channel showing dye electroporation location into LF region of NM and filled axons. **C**: Color-merge image. **D**: Schematic of C outlining NM, injection sites, and filled axons. Horizontal view; rostral is up. Scale bar = 500 μm in C (applies to A–C).

Green dye was introduced into a rostromedial (HF) portion of NM and labeled the corresponding XDCT axons (Fig. 2A); red dye was injected into a more caudolateral region that encodes a lower frequency (LF; Fig. 2B). The color-merged image and labeled axon traces are shown in Figure 2C and D, respectively. The outlines of NM are illustrated in Figure 2D. The dye injected into the rostromedial region of NM labeled a distinct set of XDCT axons decussating at a more rostral part of the midline compared to axon labeling resulting from the dye injected more caudolaterally within NM. Note that although the two injection sites are close to one another, there is a complete separation between the locations of axons labeled red or green (Fig. 2C,D).

Fluorescence intensity measurements were taken along the direction of the tonotopic axis in NM and along the rostrocaudal axis of XDCT (see Materials and Methods). Intensity measurements of dye injection locations along the NM tonotopy for eight cases are shown in Figure 3 (A,C,E,G,I,K,M,O). The x-axis represents the distance from the wall of the 4th ventricle along the NM tonotopic axis (Fig. 1B). The y-axis denotes the signal intensity normalized to span a range of 0 to 1. The corresponding intensity measurements of XDCT axon labeling along the rostrocaudal axis are shown in Figure 3 (B,D,F,H,J,L,N,P). Here, the x-axis represents the rostrocaudal distance along the midline of labeled XDCT axons (Fig. 1B), whereas the y-axis denotes the normalized signal intensity. The green dashed lines represent rostromedial (HF) dye injections, and caudolateral (LF)

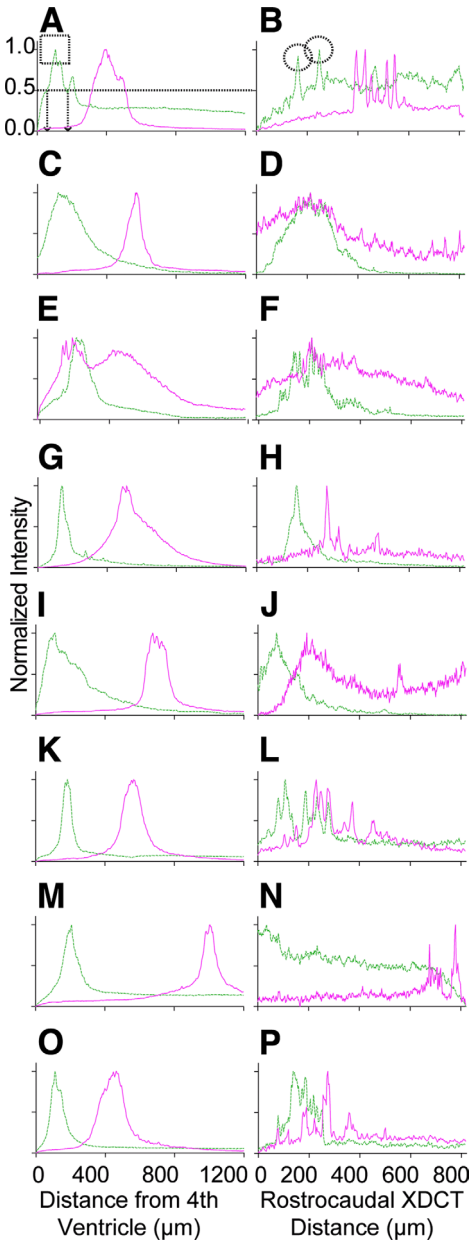

Figure 3. Normalized fluorescent intensity measurements of electroporation and filled axon locations. **A,C,E,G,I,K,M,O**: Plots of electroporation location in NM represented by normalized signal intensities versus distance from the wall of the 4th ventricle. Injection center for sample "A" is represented by the peak value (box). Injection size for sample "A" is measured through the range of values over which the intensity surpasses the value of 0.5 and is denoted by arrows. **B,D,F,H,J,L,N,P**: Plots of fluorescence intensities from filled axons along XDCT. The normalized signal intensities were measured as a function of the distance beginning where the wall of the 4th ventricle begins to curve along XDCT. Circles in B identify exemplary signal peaks corresponding to visually confirmed filled axons. Note the lack of overlap in fluorescent peaks between the two channels. For all plots, dashed green lines represent HF injection locations, and solid magenta lines represent LF injection locations. A separate letter denotes each brainstem. Sample A/B is the brainstem shown in Figure 2. [Color figure can be viewed in the online issue, which is available at wileyonlinelibrary.com.]

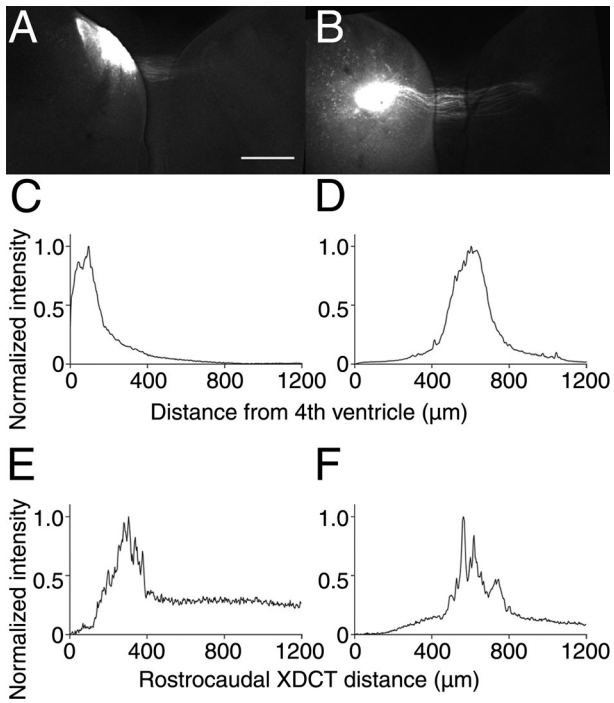

Figure 4. One-dye electroporation into NM. **A,B**: Maximum intensity projection from two cases showing the dye electroporation location and filled axons in XDCT. Horizontal view; rostral is up. **C,D**: Fluorescence intensity measurements along the NM tonotopy for A and B, respectively. **E,F**: Corresponding plots of fluorescence intensities from filled axons along XDCT. Scale bar = 500 μm in A (applies to A,B).

injections are shown as red solid lines. Figure 3A shows the measurements taken from the case shown in Figure 2. Note how separated injection centers along the NM tonotopic axis (peaks in left column) correlate with each dye labeling separate bundles of axons along the midline's rostrocaudal axis (peaks in right column). The observation that dye injections made into rostromedial and caudolateral regions of NM filled axons more rostral and caudal along the midline, respectively, was repeated with brainstems in which only one dye was injected (Fig. 4).

To quantify the relationship between the location of labeled axons along the midline rostrocaudal axis and the tonotopic position of the dye injection, we calculated the rostrocaudal distance of filled XDCT axons for each dye in the eight preparations in which two dyes were injected. Each plot in Figure 5A–H represents a single brainstem, and each point denotes the rostrocaudal location of a single labeled axon compared to the injection center in NM. Among the eight brainstems that successfully took up both dyes, all but one (Fig. 3C) had significantly different mean rostrocaudal XDCT distances for fibers filled with each dye (unpaired *t*-tests, $P < 0.05$). Comparison of NM dye injection sizes/locations revealed that all

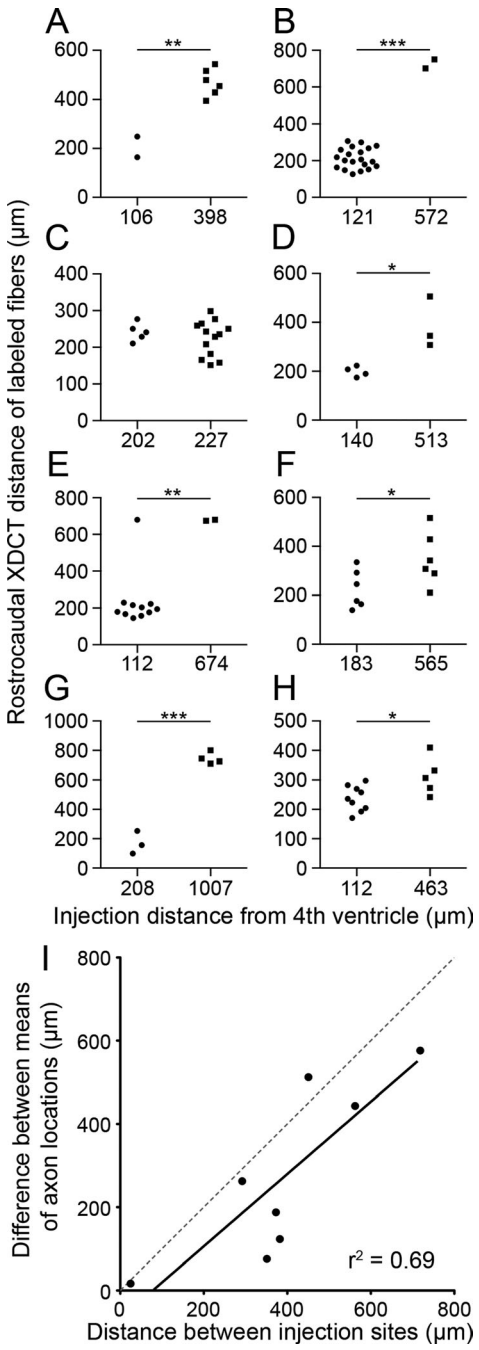

Figure 5. Rostrocaudal distance of filled XDCT axons in samples with two different-colored dyes injected into NM. **A–H**: Each graph is a separate brainstem with labels corresponding to the intensity plots shown in Figure 3. The x-axis lists the injection center location along the NM tonotopy, and the y-axis denotes the rostrocaudal midline distance where filled axons were found. For seven of the eight cases (C is the exception), the mean distances of filled axons were statistically different (unpaired *t*-test, * $P < 0.05$; ** $P < 0.005$; *** $P < 0.0001$), **I**: The distance between injection sites along the tonotopic axis in NM when two dyes were introduced is correlated with the difference between the means of corresponding labeled NM axons in XDCT (linear regression analysis, $r^2 = 0.69$, $P < 0.02$). Regression line, black line; unity line, gray dashed line. Each data point represents data from one brain.

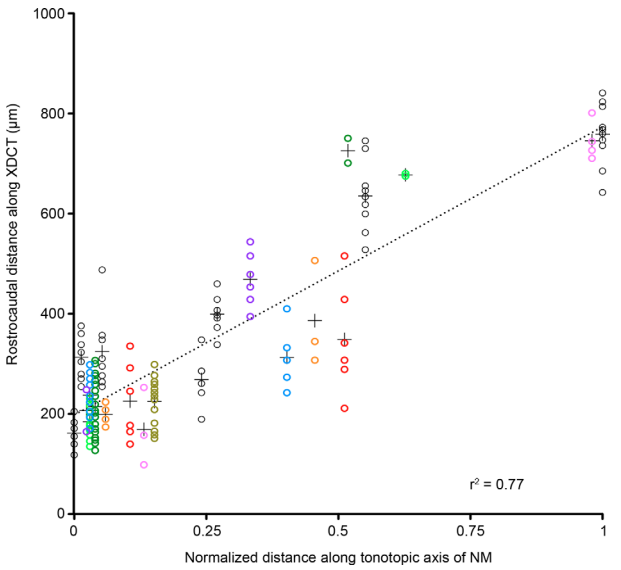

Figure 6. Correlation of injection sites and labeled axon location of all cases studied. Each circle represents the location of a single filled axon in XDCT along the rostrocaudal axis and is correlated with its corresponding injection site center along the nucleus magnocellularis (NM) tonotopic axis ($n = 15$ brainstems; 149 labeled axons). All brainstems electroporated with one dye are shown as black circles. Each brainstem electroporated with two dyes is represented as circles of a single, unique color. Crosses indicate the mean value for each dataset. The dashed line represents a linear regression of the individual axon locations and has a significant non-zero slope ($r^2 = 0.77$, $P < 0.0001$; r^2 of regression through means of axon locations: 0.80, $P < 0.0001$). Some of the data represent duplicates of the information from Figure 5.

samples except one (Figs. 3C, 5C) had 0% overlap in HF and LF dye electroporation. Moreover, the distance between the injection sites correlated with the difference between the means of the corresponding labeled axons in XDCT (Fig. 5I, $r^2 = 0.69$, $P < 0.02$).

We correlated the center of NM injection sites with the rostrocaudal location of axons labeled in XDCT for all cases (one or two dye injections, Fig. 6). These data comprise 22 NM injection sites yielding 149 labeled axons in XDCT at the midline (mean CV = 18.61%). Data obtained from brainstems filled with one dye are shown as black circles. Data from brainstems filled with two dyes are each shown as circles of varying colors. Each data point (circle) represents a single filled axon. The x-axis represents the normalized location of the injection site center along the NM tonotopic axis, and the y-axis shows the rostrocaudal distance along the midline where the corresponding labeled axons were identified. The data show a correlation between the dye electroporation location along the NM tonotopic axis and the individual locations of corresponding labeled NM axons in XDCT along the rostrocaudal axis ($r^2 = 0.77$, $P < 0.0001$).

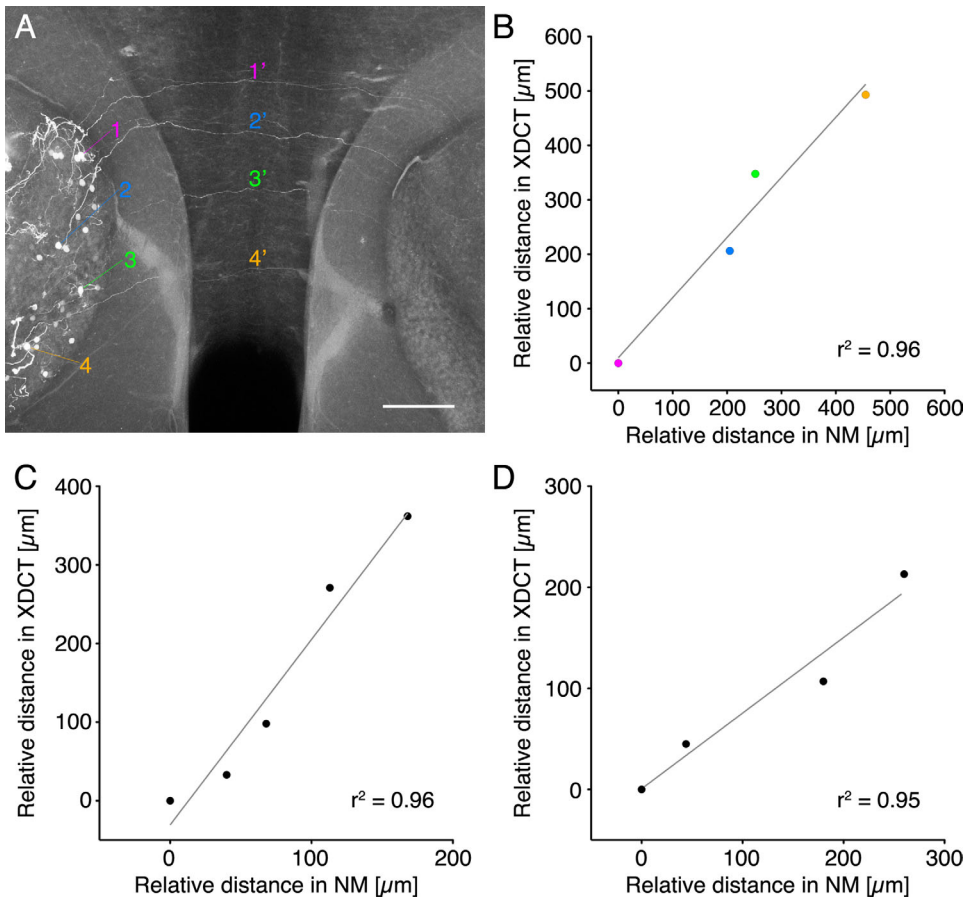

Figure 7. Correlation of single-labeled nucleus magnocellularis (NM) cells and their axons in XDCT. **A**: Montage of maximum intensity projection images showing an example whole-brainstem preparation in which several single NM neurons and their corresponding contralateral axons were labeled. View from dorsal; rostral is up. **B–D**: Correlation diagrams of the relative location of filled NM cells and the relative location of their contralateral axons in XDCT. The linear relationship indicates that the topography in NM is mirrored in the topographic arrangement of axons in XDCT. B shows the correlation of example shown in A. r^2 values depict goodness of fit of a linear regression analysis. All $P < 0.05$. Scale bar = 200 μm in A.

Multicellular injections and the corresponding axons give a clear indication of topographic relationships between soma position and axon position in XDCT. But this approach does not resolve the correlation with the same precision as can be obtained with reconstructions of single cells. We performed small injections in whole-brainstem preparations to label single NM neurons and their axons (Fig. 7, $n = 3$). Single NM cell bodies could be identified along the tonotopic axis of NM (Fig. 7A). In 3D image stacks, their contralateral axons were traced and located at the midline. The relative location of cell bodies and corresponding axons showed a linear relationship and surprisingly high correlations (Fig. 7B–D, $r^2 > 0.95$ and $P < 0.05$ for all three cases).

DISCUSSION

Axons in the auditory brainstem of the chicken projecting from nucleus magnocellularis (NM) to the contralateral nucleus laminaris (NL) are ordered in a topographic manner. It appears that the axons from neighboring NM cell bodies maintain a neighboring relationship as they cross the midline, thereby preserving the tonotopic organization of the nucleus from which they originated. This finding is not without precedence, as axons in fiber tracts of the visual and olfactory systems are arranged in a systematic manner as well. In contrast, we believe that the quantification of our results reveals a level of precision that was unexpected.

Technical considerations

We obtained our axon labeling results from E20 and E21 chicken embryos, 1 day before and day of hatching. Whether the organization of XDCT changes after hatching is unknown. However, prior studies suggest that the chicken auditory system, particularly the brain regions encoding LF sound, is developed and functional before

this age. Cochlear nuclei can exhibit sound-evoked activity beginning at E11–12, and the auditory brainstem response (ABR) thresholds to all but the highest frequencies mimic those recorded from mature birds by E20 (Saunders et al., 1973). By E19, the tonotopic map of the cochlea is essentially identical to post-hatch birds for all but the HF regions (Lippe, 1987; Jones and Jones, 1995a), and frequency tuning curves taken from the cochlear ganglion are comparable with those of mature animals (Jones and Jones, 1995b). Given this precocious nature of the chicken auditory system, we believe our results are indicative of the organization of XDCT in post-hatch birds.

Given the proximity of NM or the nearby region intermedius (RI) to NL, one methodological concern might be the accidental labeling of cells other than NM. Axons from NL project to the contralateral nucleus mesencephalicus lateralis, pars dorsalis (MLd), coursing rostrally along the lateral lemniscus following decussation along the ventral edge of the brainstem (Conlee and Parks, 1986). Axons originating from RI course rostrally and bifurcate to project to bilateral MLd (Wang and Karten, 2010). None of the brainstem preparations included in our analysis contained axons following either of these paths. This assertion was further supported through dye electroporation into the midline exclusively filling cell bodies within NM (data not shown).

Topographic axon tracts

Topographic organization of axons has been demonstrated throughout the nervous system. Examples of topographic pathways include: axon groups spanning the corpus callosum (Hofer and Frahm, 2006), functionally and anatomically differentiated components in the spinothalamic tract (Craig, 2006), and the somatotopic sciatic nerve in rats, with muscular fascicles maintaining the same relative position along the entire nerve (Badia et al., 2010). One axon pathway whose topography has been extensively studied is the retinotectal tract, comprised of the optic nerve axons that will terminate in the superior colliculus or optic tectum (Brouwer and Zeeman, 1926; Hoyt and Luis, 1962; Easter et al., 1981; Aebersold et al., 1981; Torrealba et al., 1982; Bunt and Horder, 1983; Reh et al., 1983; Voigt et al., 1983; Springer and Mednick, 1985; Naito, 1986, 1989; Fraley and Sharma, 1986; Reese and Baker, 1993; reviewed in Chelvanayagam et al., 1998). Within the optic nerve, axons exiting the retina from dorsal and ventral locations appear to maintain this spatial dimension more than axons originating from the nasal and temporal part (Simon and O'Leary, 1991; Chan and Guillery, 1994). A particularly distinct ordering of ventral versus dorsal axons was presented by Dunlop and colleagues in two species of marsupials (Chelvanayagam et al., 1998; Dunlop et al., 2000). Here, dorsal and ventral axons of the optic nerve remain organized in separate partitions throughout the whole fiber tract. A quantitative analysis of the retino-collicular axons in the mouse produced similar results (Plas et al., 2005).

Another, more recently described example of axons organized into partitions can be found in the olfactory system. In mice, axons arising from olfactory sensory neurons get sorted before they reach their target (Imai et al., 2009). The underlying axon–axon interaction causing this sorting is mediated by the axon guidance receptor Neuropilin-1 and its repulsive ligand Semaphorin-3A.

In contrast to the data noted above, axons in XDCT are not organized as a round bundle, but as a layer of fibers spanning a distance of about 1 mm along the entire rostrocaudal distance of both their origin and their target nuclei (Puelles et al., 2007; Seidl et al., 2010).

Pre-target axon sorting

Ramón y Cajal first proposed that chemical cues might serve as a prerequisite to topographic formation of neuronal connectivity (Ramón y Cajal, 1892; de Castro et al., 2007), and numerous studies have demonstrated molecular guidance of axons. Most studies addressing this issue focus on molecular cues or gradients in the origin and target regions. However, pre-target axon sorting seems to play an important role in establishing and/or maintaining topographic organization of axons. It has been speculated that the preordering of the dorsal and ventral axons in the optic nerve might deliver axons to their appropriate region of the target nucleus (Dunlop et al., 2000). Imai and colleagues (2009) showed that normal map formation fails when axons did not undergo pre-target axon sorting. Their study demonstrated that olfactory map formation was not only supported by, but also depended on, the proper sorting of olfactory sensory neuron axons along the trajectory from the sensory epithelium to the olfactory bulb.

Our results suggest a surprisingly high degree of topographic precision of NM axons at the midline as they course to the contralateral NL and form XDCT. The location of the injection site in NM and the location of the corresponding labeled fibers are highly correlated, and the distances between injection sites and resulting labeled axons also yielded a high correlation. In contrast, careful analysis of Figures 5 and 6 reveals that 31 and 23%, respectively, of the variance cannot be accounted for by a linear fit to the data, and a nonlinear analysis does not appear to be warranted. Whether this is experimental error introduced by combining data across subjects or is due to the size of the injection site, or represents inherent disorganization in the fiber plexus is impossible to determine from our dataset or from smaller injections alone. Perhaps individual NM neuron fills in nearly adjacent cells

could be done, but that is beyond the scope of this study, and additional experiments will be needed to examine whether the systematic arrangement of axons in XDCT is a necessary or sufficient prerequisite for the establishment of a tonotopic map in NL. Nevertheless, the precise and systematic ordering of axons along the midline makes it tempting to propose that no additional sorting is needed at the target in order to ensure the tonotopic connections in NL

Development of XDCT

Developing NM axons reach the brainstem midline as early as E4 (Cramer et al., 2006) and may be in the vicinity of the contralateral target region as early as E6 (Young and Rubel, 1986). Young and Rubel (1986) also showed that as early as E9, NM axon terminals are in the appropriate tonotopic locations in both the ipsilateral and the contralateral NL. It is unknown whether outgrowth of NM axons follows a particular spatial–temporal pattern related to their tonotopic location. It is hard to imagine that NM axons would initially cross the midline as an unorganized bundle and only later become arranged in a systematic manner. The axons would have to undergo substantial untangling to achieve this. Based on our findings, we can speculate that axons in XDCT are guided along their trajectory across the midline in order to maintain this arrangement.

Eph receptors and ephrins are expressed along the midline of the chicken auditory brainstem (Cramer et al., 2002), and their mis-expression in the brainstem causes aberrant wiring (Cramer et al., 2006; Huffman and Cramer, 2007). In addition, the presence of Eph/ephrin gradients was confirmed along the tonotopic axis of axon terminals onto NL (Person et al., 2004). Thus, Eph receptors and ephrins are attractive candidates for forming or maintaining the tonotopy in XDCT. A possible gradient of Eph/ephrin expression along the midline's rostrocaudal axis might guide decussating NM axons in chicken embryos between E4 and E6. Future studies will be needed to determine whether the midline expression of Ephs/ephrins in birds plays a role in establishing XDCT tonotopy.

Although Ephs/ephrins are possible factors for organizing XDCT tonotopy, other molecules may also play a role. Additional factors found to play a role in axon guidance within the developing chick include: Sonic hedgehog (Bourikas et al., 2005), Netrin-1 (MacLennan et al., 1997), Semaphorin-3A (Kubilus and Linsenmayer, 2010), Slit2 (Kubilus and Linsenmayer, 2010), and Engrailed transcription factors (Wizenmann et al., 2009).

ACKNOWLEDGMENTS

The authors thank Glen MacDonald for help with microscopy and Dale E. Cunningham for assistance with tissue processing We thank Kathryn M. Tabor, Melissa L. Caras, Jason Tait Sanchez, and R. Michael Burger for their insights and suggestions. We also thank the anonymous reviewers and the editor for their constructive criticism and comments. This project was completed as part of an undergraduate honors thesis at the University of Washington (D.T.K.).

CONFLICT OF INTEREST STATEMENT

The authors state there is no conflict of interest.

ROLE OF AUTHORS

All authors had full access to all the data in the study and take responsibility for the integrity of the data and the accuracy of the data analysis. Study concept and design: A.H.S. Acquisition of data: D.T.K., A.H.S. Analysis and interpretation of data: D.T.K., A.H.S. Drafting of the manuscript: D.T.K., A.H.S. Critical comments on the manuscript: E.W.R. Obtained funding: A.H.S., E.W.R.

LITERATURE CITED

Aebersold H, Creutzfeldt OD, Kuhnt U, Sanides D. 1981. Representation of the visual field in the optic tract and optic chiasma of the cat. Exp Brain Res 42:127–145.

Angulo A, Merchán JA, Merchán MA. 1990. Morphology of the rat cochlear primary afferents during prenatal development: a Cajal's reduced silver and rapid Golgi study. J Anat 168:241–255.

Badia J, Pascual-Font A, Vivó M, Udina E, Navarro X. 2010. Topographical distribution of motor fascicles in the sciatic-tibial nerve of the rat. Muscle Nerve 42:192–201.

Boord RL, Rasmussen GL. 1963. Projection of the cochlear and lagenar nerves on the cochlear nuclei of the pigeon. J Comp Neurol 120:463–475.

Bourikas D, Pekarik V, Baeriswyl T, Grunditz A, Sadhu R, Nardó M, Stoeckli ET. 2005. Sonic hedgehog guides commissural axons along the longitudinal axis of the spinal cord. Nat Neurosci 8:297–304.

Brouwer B, Zeeman W. 1926. The projection of the retina in the primary optic neuron in monkeys. Brain 49:1–35.

Bunt SM, Horder TJ. 1983. Evidence for an orderly arrangement of optic axons within the optic nerves of the major nonmammalian vertebrate classes. J Comp Neurol 213: 94–114.

Burger RM, Cramer KS, Pfeiffer JD, Rubel EW. 2005. Avian superior olivary nucleus provides divergent inhibitory input to parallel auditory pathways. J Comp Neurol 481: 6–18.

Carr CE, Konishi M. 1990. A circuit for detection of interaural time differences in the brain stem of the barn owl. J Neurosci 10:3227–3246.

Chan SO, Guillery RW. 1994. Changes in fiber order in the optic nerve and tract of rat embryos. J Comp Neurol 344: 20–32.

Chelvanayagam DK, Dunlop SA, Beazley LD. 1998. Axon order in the visual pathway of the quokka wallaby. J Comp Neurol 390:333–341.

Conlee JW, Parks TN. 1986. Origin of ascending auditory projections to the nucleus mesencephalicus lateralis pars dorsalis in the chicken. Brain Res 367:96–113.

Craig AD (Bud). 2006. Retrograde analyses of spinothalamic projections in the macaque monkey: input to ventral posterior nuclei. J Comp Neurol 499: 965–978.

Cramer KS, Karam SD, Bothwell M, Cerretti DP, Pasquale EB, Rubel EW. 2002. Expression of EphB receptors and EphrinB ligands in the developing chick auditory brainstem. J Comp Neurol 452:51–64.

Cramer KS, Cerretti DP, Siddiqui SA. 2006. EphB2 regulates axonal growth at the midline in the developing auditory brainstem. Dev Biol 295:76–89.

de Castro F, López-Mascaraque L, De Carlos JA. 2007. Cajal: lessons on brain development. Brain Res Rev 55: 481–489.

Dunlop SA, Tee LB, Beazley LD. 2000. Topographic order of retinofugal axons in a marsupial: implications for map formation in visual nuclei. J Comp Neurol 428:33–44.

Easter SS Jr, Rusoff AC, Kish PE. 1981. The growth and organization of the optic nerve and tract in juvenile and adult goldfish. J Neurosci 1:793–811.

Feldheim DA, O'Leary DDM. 2010. Visual map development: bidirectional signaling, bifunctional guidance molecules, and competition. Cold Spring Harb Perspect Biol 2: a001768.

Flanagan JG. 2006. Neural map specification by gradients. Curr Opin Neurobiol 16:59–66.

Fraley SM, Sharma SC. 1986. Retinal topography in the optic tract of adult goldfish. Neuroscience 19:1363–1380.

Fukui I, Ohmori H. 2004. Tonotopic gradients of membrane and synaptic properties for neurons of the chicken nucleus magnocellularis. J Neurosci 24:7514–7523.

Haas K, Sin WC, Javaherian A, Li Z, Cline HT. 2001. Single-cell electroporation for gene transfer in vivo. Neuron 29: 583–591.

Hackett JT, Jackson H, Rubel EW. 1982. Synaptic excitation of the second and third order auditory neurons in the avian brain stem. Neuroscience 7:1455–1469.

Hofer S, Frahm J. 2006. Topography of the human corpus callosum revisited—comprehensive fiber tractography using diffusion tensor magnetic resonance imaging. Neuroimage 32:989–994.

Hoyt W, Luis O. 1962. Visual fiber anatomy in the infrageniculate pathway of the primate. Arch Ophthalmol 68:94–106.

Huffman KJ, Cramer KS. 2007. EphA4 misexpression alters tonotopic projections in the auditory brainstem. Dev Neurobiol 67:1655–1668.

Imai T, Yamazaki T, Kobayakawa R, Kobayakawa K, Abe T, Suzuki M, Sakano H. 2009. Pre-target axon sorting establishes the neural map topography. Science 325: 585–590.

Jackson H, Rubel EW. 1978. Ontogeny of behavioral responsiveness to sound in the chick embryo as indicated by electrical recordings of motility. J Comp Physiol Psychol 92:682–696.

Jeffress LA. 1948. A place theory of sound localization. J Comp Physiol Psychol 41:35–39.

Jhaveri S, Morest DK. 1982a. Neuronal architecture in nucleus magnocellularis of the chicken auditory system with observations on nucleus laminaris: a light and electron microscope study. Neuroscience 7:809–836.

Jhaveri S, Morest DK. 1982b. Sequential alterations of neuronal architecture in nucleus magnocellularis of the developing chicken: a Golgi study. Neuroscience 7:837–853.

Jones SM, Jones TA. 1995a. The tonotopic map in the embryonic chicken cochlea. Hear Res 82:149–157.

Jones SM, Jones TA. 1995b. Neural tuning characteristics of auditory primary afferents in the chicken embryo. Hear Res 82:139–148.

Joseph AW, Hyson RL. 1993. Coincidence detection by binaural neurons in the chick brain stem. J Neurophysiol 69: 1197–1211.

Kandler K, Clause A, Noh J. 2009. Tonotopic reorganization of developing auditory brainstem circuits. Nat Neurosci 12: 711–717.

Kuba H, Yamada R, Fukui I, Ohmori H. 2005. Tonotopic specialization of auditory coincidence detection in nucleus laminaris of the chick. J Neurosci 25:1924–1934.

Kubilus JK, Linsenmayer TF. 2010. Developmental guidance of embryonic corneal innervation: roles of Semaphorin3A and Slit2. Dev Biol 344:172–184.

Lippe W, Rubel EW. 1985. Ontogeny of tonotopic organization of brain stem auditory nuclei in the chicken: implications for development of the place principle. J Comp Neurol 237:273–289.

Lippe WR. 1987. Shift of tonotopic organization in brain stem auditory nuclei of the chicken during late embryonic development. Hear Res 25:205–208.

MacDonald GH, Rubel EW. 2008. Three-dimensional imaging of the intact mouse cochlea by fluorescent laser scanning confocal microscopy. Hear Res 243:1–10.

MacLennan AJ, McLaurin DL, Marks L, Vinson EN, Pfeifer M, Szulc SV, Heaton MB, Lee N. 1997. Immunohistochemical localization of netrin-1 in the embryonic chick nervous system. J Neurosci 17:5466–5479.

Naito J. 1986. Course of retinogeniculate projection fibers in the cat optic nerve. J Comp Neurol 251:376–387.

Naito J. 1989. Retinogeniculate projection fibers in the monkey optic nerve: a demonstration of the fiber pathways by retrograde axonal transport of WGA-HRP. J Comp Neurol 284:174–186.

Nishino E, Ohmori H. 2009. The modulation by intensity of the processing of interaural timing cues for localizing sounds. Mol Neurobiol 40:157–165.

Overholt EM, Rubel EW, Hyson RL. 1992. A circuit for coding interaural time differences in the chick brainstem. J Neurosci 12:1698–1708.

Parks TN, Rubel EW. 1975. Organization and development of brain stem auditory nuclei of the chicken: organization of projections from n. magnocellularis to n. laminaris. J Comp Neurol 164:435–448.

Parks TN, Rubel EW. 1978. Organization and development of the brain stem auditory nuclei of the chicken: primary afferent projections. J Comp Neurol 180:439–448.

Person AL, Cerretti DP, Pasquale EB, Rubel EW, Cramer KS. 2004. Tonotopic gradients of Eph family proteins in the chick nucleus laminaris during synaptogenesis. J Neurobiol 60:28–39.

Plas DT, Lopez JE, Crair MC. 2005. Pretarget sorting of retinocollicular axons in the mouse. J Comp Neurol 491: 305–319.

Puelles L, Martinez-de-la-Torre M, Paxinos G, Watson C, Martinez S. 2007. The chick brain in stereotaxic coordinates: an atlas featuring neuromeric subdivisions and mammalian homologies. New York: Academic Press.

Ramón y Cajal S. 1892. La rétine des vertébrés. Cellule 9: 121–255.

Reese BE, Baker GE. 1993. The re-establishment of the representation of the dorso-ventral retinal axis in the chiasmatic region of the ferret. Vis Neurosci 10: 957–968.

Reh TA, Pitts E, Constantine-Paton M. 1983. The organization of the fibers in the optic nerve of normal and tectum-less *Rana pipiens*. J Comp Neurol 218:282–296.

Rubel EW, Fritzsch B. 2002. Auditory system development: primary auditory neurons and their targets. Annu Rev Neurosci 25:51–101.

Rubel EW, Parks TN. 1975. Organization and development of brain stem auditory nuclei of the chicken: tonotopic organization of n. magnocellularis and n. laminaris. J Comp Neurol 164:411–433.

Rubel EW, Parks TN. 1988. Organization and development of the avian brain-stem auditory system. In: Auditory function: neurobiological bases of hearing. New York: John Wiley & Sons. p 3–92.

Sanchez JT, Seidl AH, Rubel EW, and Barria A. 2011. Preparation and culture of chicken auditory brainstem slices. J Vis Exp e2527, doi:10.3791/2527.

Saunders JC, Coles RB, Richard Gates G. 1973. The development of auditory evoked responses in the cochlea and cochlear nuclei of the chick. Brain Res 63:59–74.

Schweitzer L, Cant NB. 1984. Development of the cochlear innervation of the dorsal cochlear nucleus of the hamster. J Comp Neurol 225:228–243.

Seidl AH, Rubel EW, Harris DM. 2010. Mechanisms for adjusting interaural time differences to achieve binaural coincidence detection. J Neurosci 30:70–80.

Simon DK, O'Leary DD. 1991. Relationship of retinotopic ordering of axons in the optic pathway to the formation of visual maps in central targets. J Comp Neurol 307:393–404.

Smith DJ, Rubel EW. 1979. Organization and development of brain stem auditory nuclei of the chicken: dendritic gradients in nucleus laminaris. J Comp Neurol 186:213–239.

Snyder RL, Leake PA. 1997. Topography of spiral ganglion projections to cochlear nucleus during postnatal development in cats. J Comp Neurol 384:293–311.

Sorensen SA, Rubel EW. 2006. The level and integrity of synaptic input regulates dendrite structure. J Neurosci 26: 1539–1550.

Springer AD, Mednick AS. 1985. Topography of the goldfish optic tracts: implications for the chronological clustering model. J Comp Neurol 239:108–116.

Torrealba F, Guillery RW, Eysel U, Polley EH, Mason CA. 1982. Studies of retinal representations within the cat's optic tract. J Comp Neurol 211:377–396.

Voigt T, Naito J, Wässle H. 1983. Retinotopic scatter of optic tract fibres in the cat. Exp Brain Res 52:25–33.

Wang Y, Karten HJ. 2010. Three subdivisions of the auditory midbrain in chicks (*Gallus gallus*) identified by their afferent and commissural projections. J Comp Neurol 518: 1199–1219.

Wizenmann A, Brunet I, Lam JSY, Sonnier L, Beurdeley M, Zarbalis K, Weisenhorn-Vogt D, Weinl C, Dwivedy A, Joliot A, et al. 2009. Extracellular Engrailed participates in the topographic guidance of retinal axons in vivo. Neuron 64: 355–366.

Yates GK, Johnstone BM, Patuzzi RB, Robertson D. 1992. Mechanical preprocessing in the mammalian cochlea. Trends Neurosci 15:57–61.

Young SR, Rubel EW. 1983. Frequency-specific projections of individual neurons in chick brainstem auditory nuclei. J Neurosci 3:1373–1378.

Young SR, Rubel EW. 1986. Embryogenesis of arborization pattern and topography of individual axons in N. laminaris of the chicken brain stem. J Comp Neurol 254:425–459.